Available online at www.sciencedirect.com

ScienceDirect

Ceramics International 40 (2014) 4127–4134

CERAMICS INTERNATIONAL

www.elsevier.com/locate/ceramint

The influence of TiO_2 content on the properties of glass ceramics: Crystallization, microstructure and hardness

Debasis Pradip Mukherjee, Sudip Kumar Das*

Department of Chemical Engineering, University of Calcutta, 92, A.P.C. Road, Kolkata 700009, India

Received 9 July 2013; received in revised form 15 August 2013; accepted 15 August 2013
Available online 22 August 2013

Abstract

The effects of compositional variation, crystallization behavior, crystalline phases and microstructure formed in the SiO_2–Al_2O_3–CaO (SAC) glass system using various amounts of TiO_2 as nucleating agent were investigated by Differential Thermal Analysis (DTA), X-ray powder diffraction (XRD), Scanning Electron Microscope (SEM), Energy-dispersive X-ray spectroscopy (EDAX) and Fourier transform infrared spectroscopy (FTIR) techniques. The crystallization kinetics and mechanical properties of SAC glass ceramics were studied using crystallization peak temperature (T_p) of three different glasses as obtained from DTA, the activation energy (E) and Avrami exponent (n) were also determined. The crystallization peak temperature (T_p) and activation energy (E) were found to increase with the increase in TiO_2 content. The major crystalline phases were anorthite and wollastonite along with gehlenite and titanite as the minor crystalline phases present in the glass ceramic system. The studies showed that the three dimensional crystalline structure and the microhardness increased with the increase of TiO_2 content in the glass ceramics system.

Keywords: B. Microstructure-final; C. Hardness; D. Glass ceramics; D. TiO_2

1. Introduction

In the glass-ceramics system the nucleating agents such as CaF_2, TiO_2 were used in order to induce bulk crystallization of the phases and to reduce the crystallization peak temperature [1–3]. Several researchers highlighted the effects of TiO_2 as a nucleating agent in mica-based glass ceramics and observed that the addition of small amount of titania had a remarkable effect on the crystallization processes [4–7]. The nature of the crystallinity and distribution of the crystalline phase(s) formed during crystallization were dependent on the type and amount of nucleating agent used [3]. Researchers had revealed that TiO_2 could be used as a good nucleating agent in many silicate systems [8,9]. Barry et al. [10] observed that the addition of TiO_2 had acted as a surface active agent and increased the nucleation rate in the LiO_2–Al_2O_3–SiO_2 (LAS) glass system. Zdaniewski [11] reported that the presence of TiO_2 in glass-ceramics system decreased the viscosity of the base glasses at high temperature, which favored the nucleation and crystal growth. The decrease in surface tension and increase in the rate of nucleation in LAS glass system by using 11.5 wt% TiO_2 as nucleating agent were reported in literature [12,13]. TiO_2, ZrO_2, and mixtures of them were used successfully to make strong spodumene glass ceramics in the LAS glass system [14,15]. Lee and Hsu [16] investigated the effects of TiO_2 in the calcium phosphate glass ceramic for biological applications. Bach and Krause [17] and Hu et al. [18] reported the use of TiO_2 as nucleating agent for making low-thermal-expansion LAS glass ceramics with a very wide range of commercial applications, like manufacturing mirrors, telescopes, cooker tops, etc. In general the sintering and crystallization parameters were strongly dependent on the composition of base glass with respect to the added nucleating agents [2].

The aim of the present work is to investigate the possible role of TiO_2 in the SiO_2–Al_2O_3–CaO glass ceramic system with respect to its nucleation, crystallization behavior, activation energy, phase separation, microstructure, microhardness and density.

*Corresponding author. Tel.: +91 9830638908.
E-mail address: drsudipkdas@vsnl.net (S.K. Das).

0272-8842/$ - see front matter © 2013 Elsevier Ltd and Techna Group S.r.l. All rights reserved.
http://dx.doi.org/10.1016/j.ceramint.2013.08.067

Table 1
Chemical composition of raw materials (in g).

Batches	CaO	Al_2O_3	SiO_2	TiO_2(% excess)
BTI	23	43	34	6
BTII	23	43	34	9
BTIII	23	43	34	12

2. Experimental procedure

2.1. Glass composition and preparation

The glass compositions with varying TiO_2 content in the SiO_2–Al_2O_3–CaO system have been studied in the present work and the detail compositions are shown in Table 1. The starting materials used were all analytical grades. Silica (SiO_2), Alumina (Al_2O_3), Calcium carbonate ($CaCO_3$) and Titanium dioxide (TiO_2) were supplied by M/S Merck Specialties Private Limited, India. Glass batches with desired compositions were mixed thoroughly in an attrition mill and thereafter, melted in an alumina crucible at 1500 °C for 2 h using electrical furnace with occasional stirring with the help of an alumina rod to make the melt homogeneous. The melted glass was then casted into a hot iron mold to form glass plates, and then annealed for 2 h at a temperature of 650 °C. The annealing conditions were so selected to avoid the nucleation at this stage. After annealing, the glass plates were cut into a number of pieces of about $50 \times 5 \times 4$ mm^3 bars. These bars were fired for nucleation in the temperature range of 730–750 °C for all the specimens (BTI, BTII and BTIII). The crystallization experiments were carried out in the temperature range of 850–1150 °C soaked for 2 h and then followed by the natural cooling to room temperature.

2.2. Characterization techniques

2.2.1. Differential thermal analysis (DTA)

The DTA measurements were performed by Differential Thermal Analyzers (Pyris Diamond TG/DTA, Perkin Elmer, Singapore) under nitrogen atmosphere (150 ml/min) at constant heating rate with α-Al_2O_3 powder as a reference material. The finely grain powdered sample (< 45 μm) of about 20 mg was placed in a platinum crucible and heated at a rate of 5 °C/min, 10 °C/min, 15 °C/min and 20 °C/min respectively from ambient temperature to 1000 °C to study the crystallization kinetics for all the samples.

2.2.2. X-ray powder diffraction analysis (XRD)

In order to determine the crystalline phases, the heat treated samples were subjected to XRD analysis (PANalytical PW3040/60, The Netherlands) using Ni filtered Cu Kα radiation at 40 kV and 30 mA setting with a scanning speed of 1°/min. The diffraction patterns were recorded within the Bragg angle range $5^\circ < 2\theta < 80^\circ$. The phases were identified by JCPDS numbers (ICDD-PDF2 data base).

2.2.3. Fourier transformed infrared spectra (FTIR)

The FTIR analysis of the heat treated samples were carried out in the range 4000–400 cm^{-1} using a fourier transform infrared spectrometer (Alpha FTIR, Bruker, Germany). The samples were ground to fine powder and then mixed with KBr powder as binder, to prepare pellets for this study.

2.2.4. Scanning electron microscopy (SEM)

SEM (FEI-QUANTA-200, the Netherland) analysis was used to identify the microstructure of the heat treated samples. The samples were prepared by polishing and then chemically etched using 10% HF solution for 15–20 s.

2.2.5. Density and microhardness measurement

The densities of ceramized glasses were measured via Archimedes's method. Micro-hardness analyses were carried out on polished glass ceramic samples using micro-indentation. Micro-indentations were taken using 160 micro-hardness testers (Carl Zeiss Jena, Germany) equipped with a conical Vickers indenter at an indent load of 40 g. Ten indents were taken for each sample with identical loading condition. The micro hardness values were calculated using the following equation for the Vickers geometry as [19,20],

$$H_v = 1.8544 \times \frac{P}{d^2} \quad (1)$$

where, H_v is the Vickers hardness number (VHN) in kg/mm^2, P is the normal load in kg, and d is the average diagonal length of the indentation in mm.

3. Results and discussion

3.1. Kinetics of crystallization

The DTA curves of three different specimens BTI, BTII and BTIII at a heating rate of 10 °C/min are shown in Fig. 1. Only one exothermic peak was observed in both BTI and BTIII specimens and this peak corresponds to the anorthite,

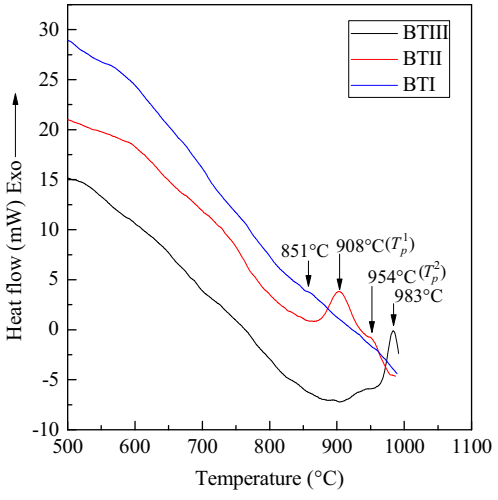

Fig. 1. DTA curves of the glass specimens BTI, BTII and BTIII at a heating rate 10 °C/min.

wollastonite and gehlenite phases. The appearance of two crystallization peaks in BTII specimen suggested that the liquid phase separation had occurred and it played an important role in both nucleation and crystallization processes. The first peak was for anorthite, gehlenite and wollastonite, and second one was for titanite. DTA results confirmed that with the increase of TiO_2 amount the crystallization peak temperature also increased. Besides this, increase of TiO_2 reduced the glass viscosity of the specimen during the melting process and it was also confirmed that incomplete melting occurred in BTI and thus reduced the crystallization peak temperature compared to the complete melted specimens in BTII and BTIII.

The activation energy (E) of crystallization was calculated using the following modified form of Kissinger equation established by Matusita and Saka [21].

$$\ln \frac{T_p^2}{\beta} = \frac{E}{RT_p} + C \tag{2}$$

where, β is the heating rate and R is the universal gas constant.

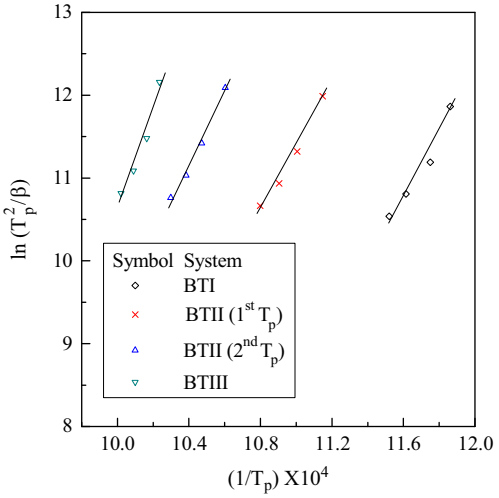

Fig. 2. Variation of $\ln(T_p^2/\beta)$ vs. $(1/T_p)$of the specimens BTI, BTII and BTIII.

The linear plots of $\ln(T_p^2/\beta)$ versus $1/T_p$ for three glass specimens are shown in Fig. 2. From the slopes of these lines the activation energy (E) was calculated for glass specimens. From the value of activation energy (E), the Avrami exponent (n) was calculated using Augis–Bennett equation [22].

$$n = \frac{2.5}{\Delta T} \times \frac{RT_p^2}{E} \tag{3}$$

where, ΔT is the full width of the exothermic DTA peak at the half maximum intensity and n is the Avrami exponent or crystallization index. The Avrami exponent (n) had indicated the nucleation and growth mechanism. According to the Johnson–Mehl–Avrami (JMA) theory, n was also related to crystallization pattern, $n \cong 2$ means that the surface crystallization dominants the overall crystallization, $n \cong 3$ means two dimensional crystallization, $n \cong 4$ means that three dimensional crystallization for bulk materials [23–25].

Table 2 shows the values of activation energy and Avrami exponents. In BTI and BTII, for first crystallization peak temperature (T_P^1), Avrami exponents were 2.44 and 2.54 respectively, which were in between 2 and 3, therefore the surface crystallization and also two dimensional crystallization played an important role in the crystallization process.

From second crystallization peak temperature (T_P^2), Avrami exponents (n) were found to be 4.02 and 3.69 for the specimens BTII and BTIII respectively (Table 2), which were close to 4, which indicated that the bulk nucleation and three dimensional crystal growth were important in crystallization process.

3.2. X-ray diffraction results

Fig. 3 represents the XRD patterns of the annealed glass specimens. It is seen that the annealed glass specimens showed the presence of unmelted particles of anorthite ($CaAl_2Si_2O_8$), wollastonite ($CaSiO_3$) and titanite ($CaTiSiO_5$) in their crystalline phases. These unmelted particles have been formed apparently

Table 2
Values of activation energy (E) and avrami exponent (n) for crystal growth of three glass specimens.

Batch no	Heating rate (β) (°C/min)	1st crystallization peak temperature (T_P^1) (K)				2nd crystallization peak temperature (T_P^2) (K)			
		T_P^1 (K)	Activation energy (kJ mole^{-1})	Avrami exponent (n)	$\langle n \rangle$	T_p^2 (K)	Activation energy (kJ mole^{-1})	Avrami Exponent (n)	$\langle n \rangle$
BTI	5	843	312.45	2.37	2.44	0	0.0	0.0	0.0
	10	851		2.41		0		0.0	
	15	861		2.46		0		0.0	
	20	868		2.53		0		0.0	
BTII	5	899	339.41	2.46	2.54	943	364.92	3.89	4.02
	10	908		2.51		954		3.99	
	15	917		2.57		963		4.06	
	20	926		2.63		971		4.13	
BTIII	5	977	511.47	3.52	3.69	0	0.0	0.0	0.0
	10	983		3.58		0		0.0	
	15	991		3.63		0		0.0	
	20	998		4.04		0		0.0	

through solids state reactions of the raw materials at the time of melting process.

Table 3 depicts the crystal phases and crystal data identified by the X-ray diffraction pattern. Fig. 4 shows the X-ray diffraction pattern for BTIII specimen heat treated at different temperature range. The peaks indicate the presence of anorthite (A) and wollastonite (W) as major phases. As temperature increases the intensity of the peaks in BTIII specimens also increases. At 850 °C, the BTII specimen was fully amorphous and the intensity of the peaks is not clearly visible. The crystallinity increases with the increase of temperature; at temperature 1050 °C onwards it was fully crystalline in nature. At higher temperature Fig. 4 clearly indicates the formation of anorthite at 21.9°, 23.3°, 27.0°, 27.8°, 31.6°, 35.9°, 43.2° and 51.5° (2θ) due to diffractions from the triclinic crystal system with space group $P\bar{1}(2)$ (cell constants $a=8.186(1)$ Å, $b=12.876(2)$ Å, $c=14.182(2)$ Å; JCPDS Card no. 70-0287) and wollastonite at 18.7°, 24.5°, 30.2°, 33.0°, 42.0° and 47.4° (2θ) due to diffractions from the triclinic crystal system with space group $P\bar{1}(2)$ ($a=7.94$ Å, $b=7.32$ Å, $c=7.07$ Å; JCPDS Card no. 76-0186) major crystalline phases with titanite (T) 49.5°, 57.4°, 59.0° and 68.1° (2θ) due to the diffractions from the monoclinic crystal system with space group $A2/a(15)$ (cell constants $a=7.077(3)$ Å, $b=8.743(4)$ Å, $c=6.584(2)$ Å; JCPDS Card no. 85-0395) and gehlenite (G) at 63.1°, 66.3° and 78.7° (2θ) due to the diffractions from the tetragonal

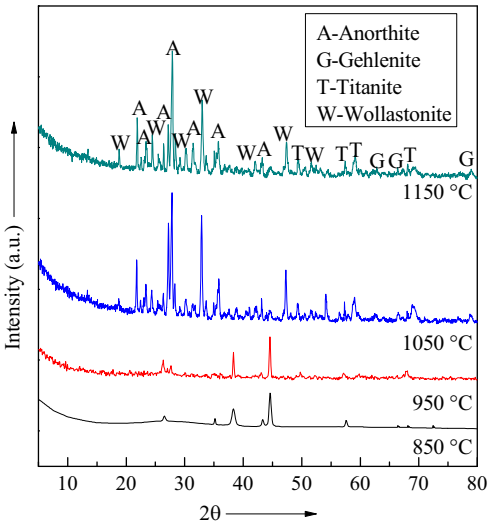

Fig. 4. XRD pattern of the specimen BTIII heat treated at different temperature soaked for 2 h.

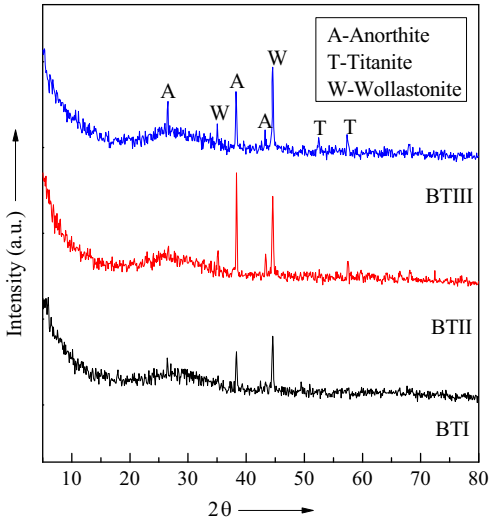

Fig. 3. XRD pattern of the glass specimens BTI, BTII and BTIII at annealing temperature.

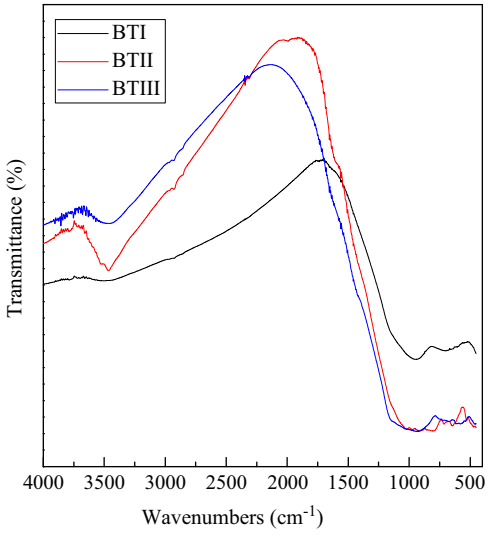

Fig. 5. FTIR spectra of glass specimens (BTI, BTII and BTIII) before heat treatment.

Table 3
Crystal phases and crystal data identified by the powder X-ray diffraction pattern.

Crystal phase	Anorthite	Gehlenite	Titanite	Wollastonite
Crystal Data				
JCPDS reference no	70-0287	79-1725	85-0395	76-0186
Chemical formula	$CaAl_2Si_2O_8$	$Ca_2Al(AlSiO_7)$	$CaTiSiO_5$	$CaSiO_3$
Molecular weight	278.21	274.20	196.06	116.16
Crystal system	Triclinic	Tetragonal	Monoclinic	Ttriclinic
Space group	$P\bar{1}(2)$	$P\bar{4}2_1m(113)$	$A2/a(15)$	$P\bar{1}(2)$
Cell parameters	$a=8.186(1)$ Å	$a=7.677(3)$ Å	$a=7.077(3)$ Å	$a=7.94$ Å
	$b=12.876(2)$ Å	–	$b=8.743(4)$ Å	$b=7.32$ Å
	$c=14.182(2)$ Å	$c=5.0594(3)$ Å	$c=6.584(2)$ Å	$c=7.07$ Å

crystal system with space group $P\bar{4}2_1m$(113)(cell constants $a=7.677(3)$ Å, $c=5.0594(3)$ Å; JCPDS Card no. 79-1725) crystal phases. Similar observations are also observed for BTI and BTII glass ceramics.

3.3. FTIR analysis results

The FTIR spectra of the specimens (BTI, BTII and BTIII) of glass and glass ceramics are shown in Figs. 5 and 6, respectively. The peak was observed at 3667 cm^{-1} which might be assigned due to the O–H vibration of the Al–OH linkage, while the peak at 3443 cm^{-1} might be due to O–H stretching vibration of the surface water and the peak at 1645 cm^{-1} might be assigned to O–H group because of bending mode of vibration of the surface. The peak at ~1666 cm^{-1} might be assigned to C=O, which was thought to originate from the CO_2 in the atmosphere. Similar type of observation was also reported in literature (3672 cm^{-1}, 3463 cm^{-1} and 1631 cm^{-1}) [26]. The peak at 1120 cm^{-1} might be due to the Al–OH vibration [27]. The band observed near at 1046 cm^{-1} corresponds to the intense Si–O and Si–O–Al stretching frequencies, characteristic of aluminosilicates [28,29]. The three intense bands appeared at around 1113, 816 and 466 cm^{-1} which was attributed to asymmetric stretching vibration of Si–O–Si bond, symmetric stretching vibration of O–Si–O bond and bending vibration of Si–O–Si bond of [SiO_4] tetrahedral unit, respectively [30–32]. The peaks at ~642 cm^{-1} did correspond to Ti–O vibration. The peak observed at 788 cm^{-1} was identified the vibration bands for TiO_6 [33]. After heat treatment at 1050 °C and 1150 °C of the specimens, the new peaks were observed at 721 cm^{-1} and 648 cm^{-1}, it might be due to the bending mode of vibration of Al–O bonds. The new peak was observed at 548 cm^{-1} is corresponding to the octahedral AlO_6 vibration [34,35].

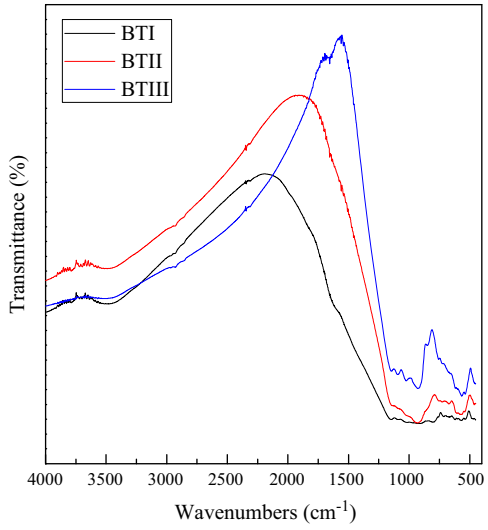

Fig. 6. FTIR spectra of glass specimens (BTI, BTII and BTIII) after heat treatment at 1150 °C temperature soaked for 2 h.

3.4. Microstructure analysis

In BTI, BTII and BTIII specimens heated at 850 °C for 2 h exhibited the presence of fine-grained microstructure [Figs. 7–9 (a)]. Specimens BTI and BTII, heat treated at 950 °C and 1050 °C for 2 h showed similar microstructure [Figs. 7 and 8 (b)–(c)]. But at 1150 °C small white spheres distributed around the glass surface was observed [Figs. 7 and 8(d)]. The results showed that with the increase of TiO_2 content, the crystallization

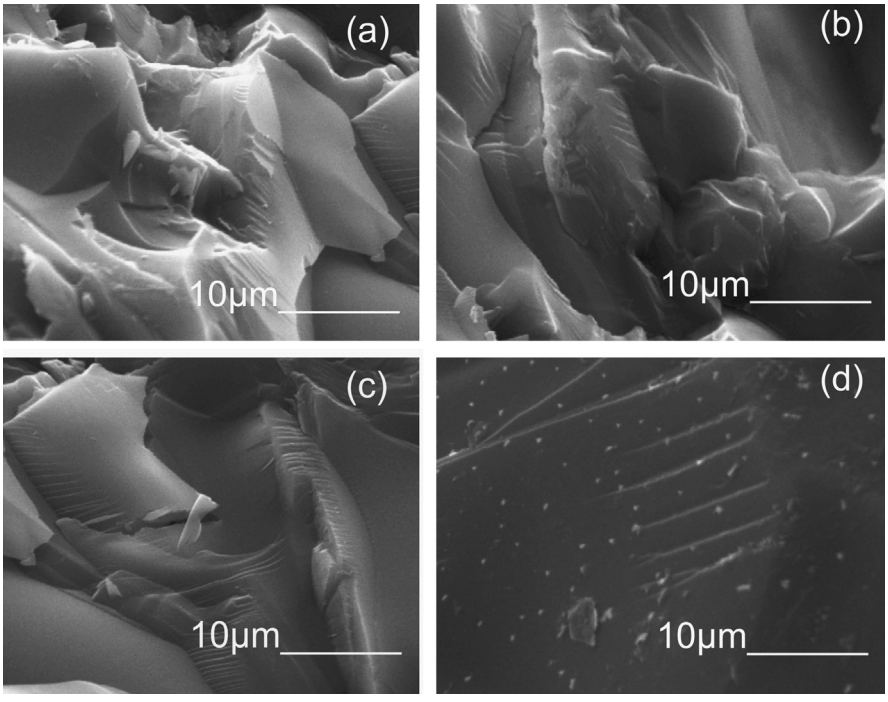

Fig. 7. (a)–(d) SEM micrograph of polished and etched surface of BTI nucleated at 750 °C for 2 h and heat treated at 850 °C (a), 950 °C (b), 1050 °C (c), and 1150 °C (d) for 2 h.

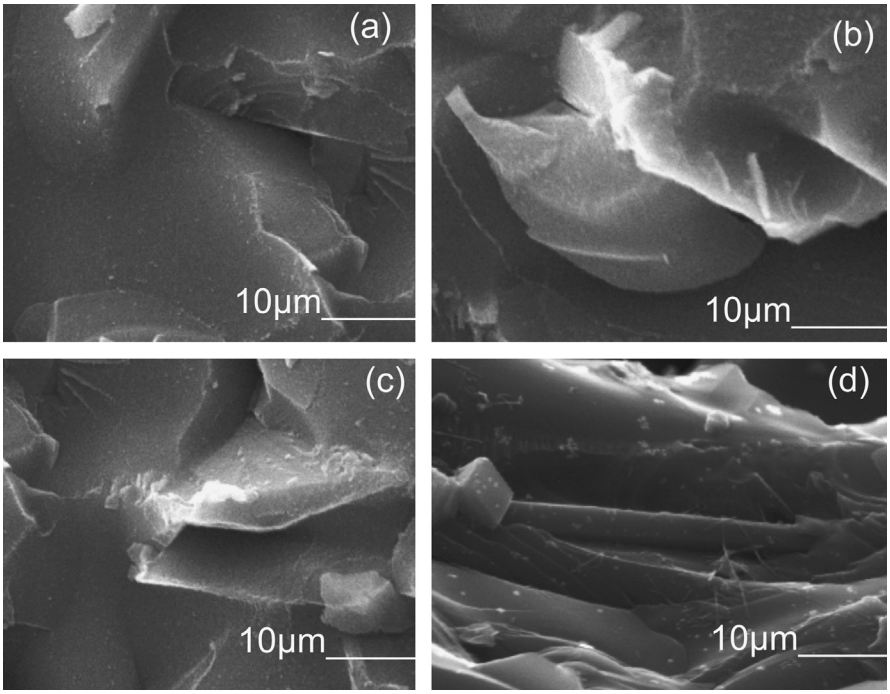

Fig. 8. (a)–(d) SEM micrograph of polished and etched surface of BTII nucleated at 750 °C for 2 h and heat treated at 850 °C (a), 950 °C (b), 1050 °C (c), and 1150 °C (d) for 2 h.

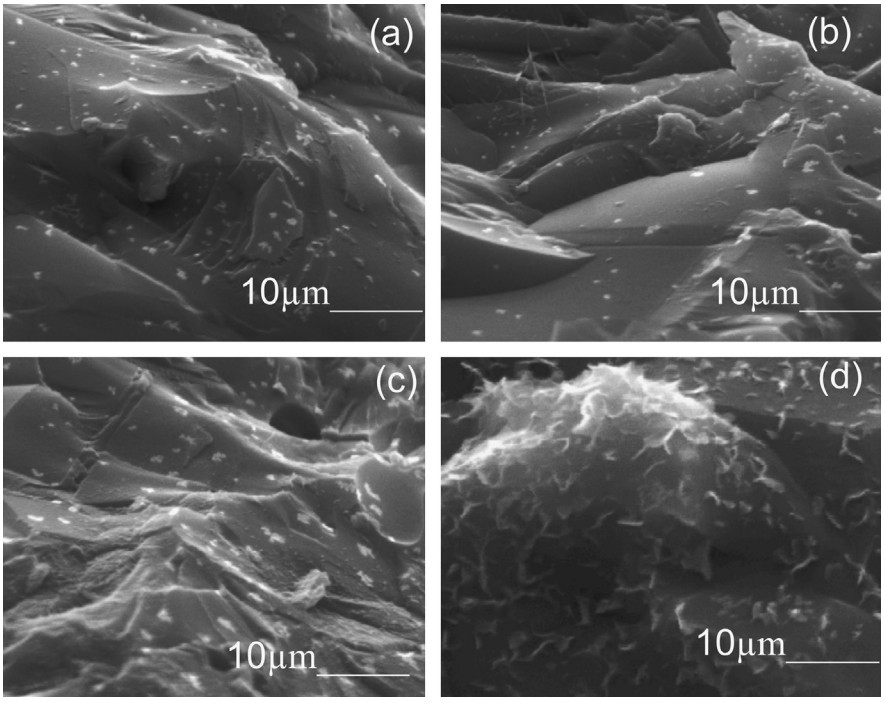

Fig. 9. (a)–(d) SEM micrograph of polished and etched surface of BTIII nucleated at 750 °C for 2 h and heat treated at 850 °C (a), 950 °C (b), 1050 °C (c), and 1150 °C (d) for 2 h.

started at higher temperature. For BTIII specimen, heat treated at 850–1050 °C temperature for 2 h showed very small white spheres like crystal structures distributed around the glass surface [Fig. 9(a–c)]. Fig. 9(d) shows that, at 1150 °C specimen BTIII was highly crystalline and the presence of TiO_2 in the glass strongly enhances volume crystallization with the formation of uniform interlocking small white spheres like morphology, titanite crystals exhibit small dendritic branches distributed around the glass surface.

Fig. 10 shows the EDAX spectrum of the glass specimen BTIII heat treated at 1150 °C for 2 h. It is to be noted that the highest peak belongs to Al and Ca in the EDAX analysis. It is

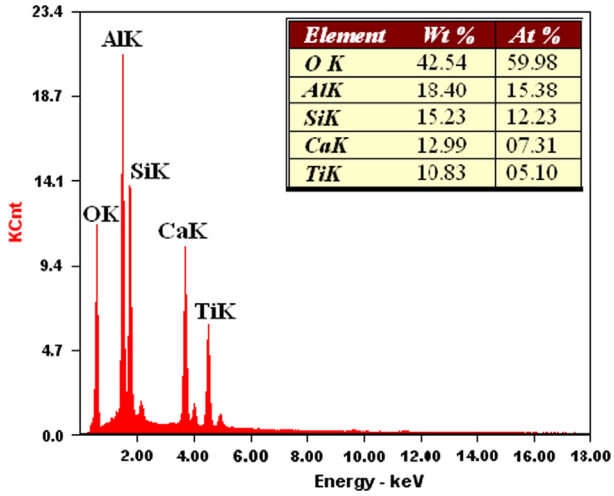

Fig. 10. EDAX spectrum of the glass specimen BTIII heat treated at 1150 °C for 2 h.

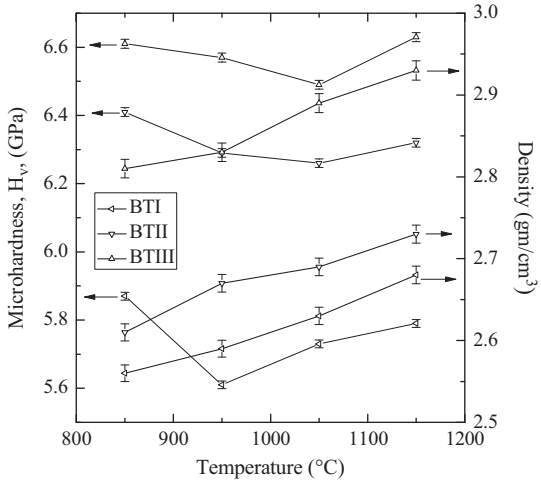

Fig. 11. Variation of Vickers hardness (H_v) and Density with different heat treatment temperature for BTI, BTII and BTIII specimens.

Table 4
Microhardness and density of glass ceramics batches with different.

Batch no	Heat treatment temperature (°C)	Microhardness (H_v) in GPa	Density (g/cm^3)
BTI	850	5.87 ± 0.01	2.56 ± 0.01
	950	5.61 ± 0.01	2.59 ± 0.01
	1050	5.73 ± 0.01	2.63 ± 0.01
	1150	5.79 ± 0.01	2.68 ± 0.01
BTII	850	6.41 ± 0.01	2.61 ± 0.01
	950	6.29 ± 0.01	2.65 ± 0.01
	1050	6.26 ± 0.01	2.69 ± 0.01
	1150	6.32 ± 0.01	2.73 ± 0.01
BTIII	850	6.61 ± 0.01	2.81 ± 0.01
	950	6.57 ± 0.01	2.83 ± 0.01
	1050	6.49 ± 0.01	2.89 ± 0.01
	1150	6.63 ± 0.01	2.93 ± 0.01

observed that the anorthite and wollastonite crystalline phases are present in all the batches.

3.5. Density and microhardness measurement analysis results

The densities of all specimens of glass ceramics are listed in Table 4. It is clear from the table that as the amount of TiO_2 content increases the density increases and also with the increase of heat treated temperature (Fig. 11). The increase in density might be attributed due to the formation of titanite crystalline phase, which exhibits small dendritic branches distributed around the glass surface during the crystal growth process by heat treated at maximum temperature, 1150 °C.

The microhardness for the glass ceramics specimens are presented in Table 4 and shown in Fig. 11. As the heat treated temperature increases from 850 °C to 1050 °C, the hardness values gradually decreases for BTII and BTIII specimens. At 1150 °C, the hardness values increased slightly for all the specimens. At any particular temperature, the microhardness values increased with increase in TiO_2 content as the titanite phase increases.

4. Conclusions

The influences of different TiO_2 content on the crystallization of SiO_2–Al_2O_3–CaO system of glass ceramics were investigated.

1. Addition of TiO_2 to the SiO_2–Al_2O_3–CaO glass system can promote crystallization. As TiO_2 content increases, both the crystallization peak temperature (T_p) and activation energy (E) were found to increase and the value of the Avrami exponent (n) reached its highest point.
2. The XRD and FTIR analysis result indicated that the main crystalline phases were anorthite and wollastonite along with the minor crystalline phases was gehlenite and titanite.
3. As the TiO_2 content increased the glass system showed higher crystal volume fraction as well as uniform interlocking arrangement in their crystal structure.
4. Three dimensional and homogeneous crystal growths were observed with the increase of the TiO_2 content in the prepared glass ceramics.

The prepared glass ceramic with highest (12%) TiO_2 content showed good mechanical properties with hardness of 6.63 GPa and density of 2.93 g/cm^3.

Acknowledgments

The authors would like to thank the UPE scheme of University Grants Commission and the Center for Research in Nanoscience and Nanotechnology (CRNN), University of Calcutta for financial support. One of the authors, Debasis Pradip Mukherjee thanks the Center for Research in Nanoscience and Nanotechnology (CRNN), University of Calcutta, Kolkata, India, for providing the fellowship.

References

[1] V. Vogel, in: Glass Chemistry, Springer-Verlag, Berlin, 1994.
[2] C.L. Lo, J.G. Duh, B.S. Chiou, W.H. Lee, Microstructure characteristics for anorthite composite glass with nucleating agents of TiO_2 under non-isothermal crystallization, Materials Research Bulletin 37 (2002) 1949–1960.

[3] D.P. Mukherjee, S.K. Das, SiO_2–Al_2O_3–CaO glass ceramics: effects of CaF_2 on crystallization, microstructure and properties, Ceramics International 39 (2013) 571–578.
[4] J.J. Shyu, J.M. Wu, Effect of TiO_2 addition on the nucleation of apatite in an MgO–CaO–SiO_2–P_2O_5 glass, Journal of Materials Science Letters 10 (1991) 1056–1058.
[5] P.W. Macmillan, in: Glass-ceramics, 2nd edition, Academics Press, London, New York, San Francisco, 1979.
[6] S. Taruta, K. Watanabe, K. Kitajima, N. Takusagawa, Effect of titania addition on crystallization process and some properties of calcium mica–apatite glass ceramics, Journal of Non-Crystalline Solids 321 (1–2) (2003) 96–102.
[7] Y.M. Sung, J.S. Lee, K.C. Shin, The role of precursor nuclei in the crystallization of aluminosilicate glasses, Journal of Materials Science Letters 19 (2000) 675–677.
[8] M. Rezvani, B. Eftekhari-Yekta, M. Solati-Hashjin, K. Marghussian, Effect of Cr_2O_3, Fe_2O_3 and TiO_2 nucleants on the crystallization behaviour of SiO_2–Al_2O_3–CaO–MgO(R_2O) glass-ceramics, Ceramics International 31 (2005) 75–80.
[9] C.H. Gur, A. Ozturk, Determination of the influence of TiO_2 on the elastic properties of a mica based glass ceramic by ultrasonic velocity measurements, Journal of Non-Crystalline Solids 351 (46–48) (2005) 3655–3662.
[10] T.I. Barry, D. Clinton, L.A. Lay, R.A. Mercer, R.P. Miller, Crystallization of glasses based on eutectic compositions in the system Li_2O–Al_2O_3–SiO_2, Journal of Materials Science 5 (2) (1970) 117–126.
[11] W. Zdaniewski, DTA X-Ray, Analysis study of nucleation and crystallization of MgO–Al_2O_3–SiO_2 glasses containing ZrO_2, TiO_2, and CeO_2, Journal of the American Ceramic Society 58 (5–6) (1975) 163–169.
[12] S.D. Stookey, Method of making ceramics and product thereofus, Patent 2920971, 1960.
[13] T.I. Barry, L.A. Lay, R. Morrell, Proceedings of the British Ceramic Society 22 (1973) 27.
[14] D.R. Stewart, in: Advances in Nucleation and Crystallization in Glasses, American Ceramic Society, Columbus (1971) 83.
[15] H. Scheidler, W. Sack, Proceedings of the IXth International Congress on Glass, Institut du Verre (International Congress on Glass, Paris, 1971), 1971, p. 1064.
[16] J.S. Lee, C.K. Hsu, The devitrification behavior of calcium phosphate glass with TiO_2 addition, Thermochimica Acta 333 (1999) 115–119.
[17] H. Bach, D. Krause, in: Low Thermal Expansion Glass-Ceramics, 2nd Edition, Springer-Verlag, Berlin Heidelberg (2005) 25–41.
[18] A. Hu, M. Li, D. Mao, Controlled crystallization of glass-ceramics with two nucleating agents, Materials Characterization 60 (2009) 1529–1533.
[19] B.R. Lawn, D.B. Marshall, Hardness, toughness, and brittleness: an indentation analysis, Journal of the American Ceramic Society 62 (1979) 347–350.
[20] I.W. Donald, R.A. McCurrie, Microstructure and indentation hardness of an MgO–LiO_2–Al_2O_3–SiO_2–TiO_2 glass-ceramics, Journal of the American Ceramic Society 55 (1972) 289–291.
[21] K. Matusita, S. Saka, Kinetic study of crystallization of glass by differential thermal analysis-criterion on application of Kissinger plot, Journal of Non-Crystalline Solids 39 (1980) 741–746.
[22] J.A. Augis, J.E. Bennett, Calculation of the Avrami parameters for heterogeneous solid state reactions using a modification of the Kissinger method, Journal of Thermal Analysis 13 (1978) 283–292.
[23] K. Cheng, Evaluation of crystallization kinetics of glasses by non-isothermal analysis, Journal of Materials Science 36 (2001) 1043–1048.
[24] Y.J. Park, J. Heo, Nucleation and crystallization kinetics of glass derived from incinerator fly ash waste, Ceramics International 28 (6) (2002) 669–673.
[25] L.A. Perez-Maqueda, J.M. Criado, J. Malek, Combined kinetics analysis for crystallization kinetics of non-crystallization solid, Journal of Non-Crystalline Solids 320 (1–3) (2003) 84–91.
[26] S.S. Amritphale, N. Chandra, R. Kumar, Sintering behaviour of pyrophyllite mineral: effect of some alkali and alkaline earth metal carbonates, Journal of Materials Science 27 (1992) 4797–4804.
[27] J.G. Miller, An infrared spectroscopic study of the isothermal dehydroxylation of kaolinite at 470 8C, Journal of Physical Chemistry 65 (5) (1961) 800–804.
[28] S. Raman, T.K. Dan, Physico chemical analysis of a raw brick clay of Bhopal (M.P.), Indian Ceramics 29 (2) (1986) 25–27.
[29] A.E. Lavat, M.C. Grasselli, J.E. Tasca, Phase changes of ceramic whiteware slip-casting bodies studied by XRD and FTIR, Ceramics International 33 (6) (2007) 1111–1117.
[30] P. Saravanapavan, L.L. Hench, Mesoporous calcium silicate glasses. I. Synthesis, Journal of Non-Crystalline Solids 318 (1-2) (2003) 1–13.
[31] A. Martı´nez, I. Izquierdo-Barba, M. Vallet-Regi, Bioactivity of a CaO–SiO_2 binary glasses system, Chemistry of Materials 12 (2000) 3080–3088.
[32] I. Izquierdo-Barba, A.J. Salinas, M. Vallet-Regí, In vitro calcium phosphate layer formation on sol-gel glasses of the CaO–SiO_2 system, Journal of Biomedical Materials Research 47 (2) (1999) 243–250.
[33] C.W. Brown, Rhode Island, Mid-IR and Rama non line spectroscopy, what are the differences K.D.O Jackson, Internet Journal of Vibrational Spectroscopy 2 (3) (1999).
[34] K. Ramaswamy, M. Kamalakkan, Infrared study of some south Indian clays, Indian Journal of Pure and Applied Physics 25 (4) (1987) 284–286.
[35] S. Bhattacharyya, A. Ghatak, Synthesis and characterization of YAG precursor powder in the hydroxygel form, Ceramics International 35 (1) (2009) 29–34.